Polyhedron 38 (2012) 275–284

Contents lists available at SciVerse ScienceDirect

Polyhedron

journal homepage: www.elsevier.com/locate/poly

Towards a selective cytotoxic agent for prostate cancer: Interaction of zinc complexes of polyhydroxybenzaldehyde thiosemicarbazones with topoisomerase I

Kong Wai Tan [a], Hoi Ling Seng [b], Fei Shen Lim [c], Shiau-Chuen Cheah [d], Chew Hee Ng [c], Kong Soo Koo [c], Mohd. Rais Mustafa [d], Seik Weng Ng [a], Mohd. Jamil Maah [a,*]

[a] Department of Chemistry, University of Malaya, 50603 Kuala Lumpur, Malaysia
[b] School of Science and Engineering, Malaysia University of Science and Technology, 47301 Selangor, Malaysia
[c] Faculty of Science, University Tunku Abdul Rahman, 31900 Kampar, Perak, Malaysia
[d] Department of Pharmacology, University Malaya, 50603 Kuala Lumpur, Malaysia

ARTICLE INFO

Article history:
Received 22 February 2012
Accepted 8 March 2012
Available online 15 March 2012

Keywords:
Cytotoxicity
Schiff base
Topoisomerase I
Prostate cancer
Zinc
Thiosemicarbazone

ABSTRACT

Four thiosemicarbazones ligands, $H_3T(1)$, $H_3M(2)$, $H_3E(3)$ and $H_3P(4)$ have been prepared with good yield by refluxing 2,4-dihydroxybenzaldehyde with N(4)-substituted thiosemicarbazide in ethanol ($H_3T(1)$ = 2,4-dihydroxybenzaldehyde thiosemicarbazone; $H_3M(2)$ = 2,4-dihydroxybenzaldehyde 4-methylthiosemicarbazone; $H_3E(3)$ = 2,4-dihydroxybenzaldehyde 4-ethylthiosemicarbazone and $H_3P(4)$ = 2,4-dihydroxybenzaldehyde 4-phenylthiosemicarbazone). Reactions of these ligands with zinc acetates in the presence of 2,2′-bipyridine lead to the formation of zinc(II) complexes of formulation [Zn(bpy)L](5–8) (bpy = 2,2′-bipyridine; L = doubly deprotonated thiosemicarbazones = HT(5); HM(6); HE(7) and HP(8)). These compounds were characterized and their cytotoxicity and topoisomerase I inhibition activities studied. X-ray diffraction study indicates that complex **8** is five coordinated and the coordination geometry around zinc(II) is trigonal bipyramidal distorted square based pyramid (TBDSBP). The doubly deprotonated thiosemicarbazone acts as a tridentate ONS-donor ligand while 2,2-bipyridne as the NN-donor ligand. Complexes **6**, **7** and **8** are more cytotoxic towards PC3 (prostate cancer cell line) than RWPE-1 (prostate normal cell line). The cytotoxicity and topoisomerase I inhibition activities seem to be dependent on the N(4) substituent of the thiosemicarbazone moiety.

1. Introduction

Thiosemicarbazones are a class of Schiff bases that have been evaluated for various biological properties such as anticancer, antimicrobial and antiviral properties [1]. Research on the biological properties of thiosemicarbazones, as well as on those of their metal complexes, has recently revealed the abilities of these compounds to act as ribonucleotide reductase, [2] topoisomerase, [3] and proteasome [4] inhibitors. In particular, the metal complexes of salicylaldehyde N^4-substituted thiosemicarbazones have been most studied [5]. On the other hand, the polyhydroxybenzaldehyde thiosemicarbazones derivatives have been less studied [6].

As the metal ions themselves are Lewis acceptors, the coordination chemistry of their adducts, particularly with *N*-heterocycles, can yield information on the mode of biological activity. A suitable metal for this purpose is zinc, whose ion is involved in many enzymatic reactions and is relatively less toxic compared with other metal ions [7]. Furthermore, zinc is known to play an important role in maintaining a healthy prostate. Clinical and experimental evidence for the last 50 years show that zinc is markedly decreased in prostate cancer [8]. On top of that, zinc is also known to enhance antitumor activity of thiosemicarbazones. For example, the IC_{50} value for (1E)-1-pyridin-2-ylethan-1-one thiosemicarbazone (HAcTsc) against the MCF-7 cell line is 3.29 μM and for the zinc(II) complexes of HAcTsc, the IC_{50} value is 1.36 and 0.88 μM for [$ZnCl_2$(HAcTsc)] and [$Zn(AcTsc)_2$], respectively [9].

Therefore in our attempt to develop a new class of selective prostate cancer targeting metal-based drug, the cytotoxicity of four new zinc complexes of N(4) substituted thiosemicarbazones were evaluated towards cancerous and normal prostate cells. Compounds with different N(4) substituent were chosen because antineoplastic activity of thiosemicarbazones are highly dependent on the substituent at the N(4) position. For example, palladium(II) complex of 2-benzoylpyridine thiosemicarbazone with a phenyl substituent at the N(4) is the most cytostatic compared to the methyl substituted and non-substituted derivatives [10]. In order to gain a better insight on the possible mode of action of these potentially cytotoxic compounds, their interaction with topoisomerase I is also reported herein.

* Corresponding author.
E-mail address: mjamil@um.edu.my (M.J. Maah).

0277-5387/$ - see front matter © 2012 Elsevier Ltd. All rights reserved.
http://dx.doi.org/10.1016/j.poly.2012.03.014

2. Experimental

2.1. Materials and solutions

The solvents were purchased from Merck and the reactants for syntheses were from Sigma. The pBR322, gene ruler 1 kb DNA ladder, 6× loading buffer and Tris-(hydroxymethyl)aminomethane (Tris) were procured from BioSyn Tech (Fermentas). Analytical grade agarose powder was obtained from Promega. Sodium chloride, human DNA topoisomerase I and ethidium bromide were purchased from Sigma Chemical Co. (USA). The aqueous solutions for DNA experiments were prepared with ultra-pure water from an Elga PURELAB ULTRA Bioscience water purification system with a UV light accessory. The Tris–NaCl (TN) buffer was prepared from the combination of Tris base and NaCl dissolved in water and its pH was adjusted with hydrochloric acid (HCl) solution to pH 7.5. The Tris–NaCl buffer pH 7.5 contains Tris at 5 mM and NaCl at 50 mM. All the test compounds in *N*,*N*-dimethylformamide (DMF) were freshly prepared daily.

2.2. Physical measurements

IR spectra were recorded as KBr pellets by using a Perkin-Elmer Spectrum RX-1 spectrophotometer. NMR spectra were recorded in deuterated DMSO-d_6 on a JEOL JNM-LA400 or ECA 400 MHz instrument. Elemental analyses were performed on a Thermo Finnigan Eager 300 CHNS elemental analyzer. UV–Vis spectroscopic measurements were carried out on a Perkin-Elmer Lambda 40 spectrophotometer.

2.3. Syntheses

2.3.1. Synthesis of 2,4-dihydroxybenzaldehyde thiosemicarbazone, H_3T (**1**)

The ligand was synthesized by minor modification to the procedure reported by Zhu et al. [6]. Thiosemicarbazide (0.09 g, 1 mmol) and 2,4-dihydroxybenzaldehyde (0.14 g, 1 mmol) were heated in an ethanol/water mixture (20/5 ml) for 3 h. Slow evaporation of the solvent yielded yellow crystals. The crystals were filtered, washed with cold methanol and ether, dried in air and kept in a desiccator over silica gel.

Yield: 0.18 g, 85%. *Anal.* Calc. for $C_8H_9N_3O_2S$: C, 45.49; H, 4.29; N, 19.89. Found: C, 45.98; H, 3.94; N, 20.01%. IR (KBr disc, cm^{-1}): 3478 m, 3342 m, 3174 s, 2997 w, 1625 s, 1555 s, 1507 s, 1379 m, 1317 m, 1287 m, 1239 s, 1165 s, 1122 s, 864 m, 810 m, 792 m, 482 m, 452 m (s, strong; m, medium; w, weak).

Characteristic ^{1}H NMR signals (DMSO-d_6, TMS, ppm): 11.49 (s, 1H, NHCS), 9.75 (s, 2H, OH), 8.20 (s, 1H, CH=N), 7.92 (s, 1H, NH_2), 7.71 (s, 1H, NH_2), 7.64 (d, 1H, aromatic, J = 8 Hz), 6.26 (s, 1H, aromatic), 6.21 (d, 1H, aromatic, J = 8 Hz). Characteristic ^{13}C NMR signals (DMSO-d_6, TMS, ppm): 177.40 (C=S), 161.04 (C–O), 158.56 (C–O), 140.97 (C=N), 128.67, 112.11, 108.26, 102.80 (C-aromatic).

2.3.2. Synthesis of 2,4-dihydroxybenzaldehyde 4-methylthiosemicarbazone, H_3M (**2**)

Similar to the preparation of **1**.

Yield: 0.20 g, 89%. *Anal.* Calc. for $C_9H_{11}N_3O_2S$: C, 47.99; H, 4.92; N, 18.65. Found: C, 48.28; H, 5.21; N, 18.98%. IR (KBr disc, cm^{-1}): 3342 m, 3249 m, 3127 w, 1625 s, 1573 s, 1521 m, 1459 w, 1331 s, 1270 m, 1231 s, 1166 m, 1125 m, 1019 m, 967 w, 868 m, 817 m, 780 w, 670 m, 635 m, 586 w, 547 w, 497 w, 374 w (s, strong; m, medium; w, weak).

Characteristic ^{1}H NMR signals (DMSO-d_6, TMS, ppm): 11.18 (s, 1H, NHCS), 9.88 (s, 1H, OH), 9.74 (s, 1H, OH), 8.20 (s, 1H, CH=N), 8.24 (d, 1H, N*H*CH_3, J = 4 Hz), 7.68 (d, 1H, aromatic, J = 8 Hz), 6.26 (s, 1H, aromatic), 6.24 (d, 1H, aromatic, J = 8 Hz), 2.95 (d, 3H, NCH_3, J = 4 Hz). Characteristic ^{13}C NMR signals (DMSO-d_6, TMS, ppm): 177.61 (C=S), 160.87 (C–O), 158.40 (C–O), 140.54 (C=N), 128.67, 112.45, 108.19, 102.80 (C-aromatic), 31.28 (N-CH_3).

2.3.3. Synthesis of 2,4-dihydroxybenzaldehyde 4-ethylthiosemicarbazone, H_3E (**3**)

Similar to the preparation of **1**.

Yield: 2.05 g, 86%. *Anal.* Calc. for $C_{10}H_{13}N_3O_2S$: C, 50.19; H, 5.48; N, 17.56. Found: C, 50.32; H, 5.28; N, 17.78%. IR (KBr disc, cm^{-1}): 3382 m, 3295 m, 3163 s, 2979 w, 1626 s, 1579 m, 1551 s, 1499 s, 1401 m, 1302 s, 1241 s, 1166 s, 1126 m, 1099 m, 938 w, 867 w, 820 w, 801 w, 741 w, 642 w, 621 w, 522 m (s, strong; m, medium; w, weak).

11.16 (s, 1H, NHCS), 9.76 (s, 2H, OH), 8.26 (s, 1H, CH=N), 8.31 (d, 1H, N***H***CH_2–, J = 4 Hz), 7.72 (d, 1H, aromatic, J = 8 Hz), 6.32 (s, 1H, aromatic), 6.30 (d, 1H, aromatic, J = 8 Hz), 3.57 (m, 2H, NC***H***$_2$–, J = 4 Hz) 1.14 (d, 3H, NCH_2C***H***$_3$, J = 4 Hz). Characteristic ^{13}C NMR signals (DMSO-d_6, TMS, ppm): 176.34 (C=S), 160.84 (C–O), 158.40 (C–O), 140.99 (C=N), 128.88, 112.34, 108.32, 102.81 (C-aromatic), 32.20 (N-**C**H_2–), 15.21 (NCH_2***C***H_3).

2.3.4. Synthesis of 2,4-dihydroxybenzaldehyde 4-phenylthiosemicarbazone, H_3P (**4**)

Similar to the preparation of **1**.

Yield: 0.23 g, 80%. *Anal.* Calc. for $C_{14}H_{13}N_3O_2S$: C, 58.52; H, 4.56; N, 14.62. Found: C, 58.38; H, 4.26; N, 14.29%. IR (KBr disc, cm^{-1}): 3331 m, 3144 m, 2974 m, 1629 s, 1542 s, 1223 m, 1264 s, 1210 s, 1121 s, 978 m, 838 w, 743 w, 694 w (s, strong; m, medium; w, weak).

Characteristic ^{1}H NMR signals (DMSO-d_6, TMS, ppm): 11.54 (s, 1H, NHCS), 9.93 (s, 1H, OH), 9.89 (s, 1H, OH), 8.72 (s, 1H, N**H**C_6H_5), 8.34 (s, 1H, CH=N), 7.82 (d, 1H, aromatic, J = 8 Hz), 7.53 (d, 2H, aromatic, J = 8), 7.33 (t, 2H, aromatic, J = 8), 7.16 (t, 1H, aromatic, J = 8), 6.29 (s, 1H, aromatic), 6.27 (d, 1H, aromatic, J = 4 Hz). Characteristic ^{13}C NMR signals (DMSO-d_6, TMS, ppm): 175.57 (C=S), 161.21 (C–O), 158.75 (C–O), 141.73 (C=N), 139.64, 129.25, 126.06, 125.66, 112.23, 108.38, 102.84 (C-aromatic).

2.3.5. Synthesis of (4-hydroxy-2-oxidobenzaldehyde thiosemicarbazonato)-(2,2′-bipyridine)zinc(II), [Zn(bipy)(HT)] (**5**)

Zinc acetate dihydrate (0.22 g, 1 mmol) and 2,2′-bipyridine (0.16 g, 1 mmol) were heated in ethanol (20 ml) for 1 h followed by addition of 2,4-dihydroxybenzaldehyde thiosemicarbazone, H_3T (0.21 g, 1 mmol) in hot ethanol (20 ml) and the mixture was refluxed for another 3 h. The yellow complex that formed was filtered, washed with cold methanol and ether, dried in air and kept in a desiccator over silica gel. Yield: 0.28 g, 65%. *Anal.* Calc. for $C_{18}H_{15}N_5O_2SZn$: C, 50.18; H, 3.51; N, 16.26. Found: C, 50.43; H, 3.26; N, 16.54%. IR (KBr disc, cm^{-1}): 3428 w, 3316 m, 3142 w, 3070 w, 3069 w, 1604 s, 1478 s, 1444 m, 1315 m, 1252 m, 1219 s, 1175 s m, 1122 m, 842 w, 763 m, 553 w, 420 w (s, strong; m, medium; w, weak).

Characteristic ^{1}H NMR signals (DMSO-d_6, TMS, ppm): 9.47 (s, broad, 1H, OH), 8.62 (d, 2H, bipy, J = 4 Hz), 8.42 (d, 2H, bipy, J = 8 Hz), 8.18 (s, 1H, CH=N), 7.98 (t, 2H, bipy, J = 8 Hz), 7.48 (d, 2H, bipy, J = 4 Hz), 6.92 (s, broad, 1H, aromatic), 6.30 (s, broad, 1H, aromatic), 6.02 (s, broad, 1H, aromatic + 2H, –N**H**$_2$).

2.3.6. Synthesis of (4-hydroxy-2-oxidobenzaldehyde 4-methylthiosemicarbazonato)-(2,2′-bipyridine)zinc(II) trihydrate, [Zn(bipy)(HM)]·3H_2O (**6**)

Similar to the preparation of **5**.

Yield: 0.40 g, 80%. *Anal.* Calc. for $C_{19}H_{23}N_5O_5SZn$: C, 45.74; H, 4.65; N, 14.04. Found: C, 4.53; H, 4.21; N, 13.59%. IR (KBr disc,

cm^{-1}): 3378 m (broad), 3236 m, 3075 w, 1602 s, 1441 m, 1405 m, 1332 m, 1273 m, 1220 m, 1175 m, 849 w m, 765 m, 652 w, 551 w, 450 w (s, strong; m, medium; w, weak).

Characteristic ^{1}H NMR signals (DMSO-d_6, TMS, ppm): 8.54 (s, 2H, bipy), 8.45 (d, 2H, bipy, J = 8 Hz), 8.27 (s, 1H, CH=N), 8.05 (s, broad, 2H, bipy), 7.57 (s, broad, 2H, bipy), 6.94 (d, 1H, aromatic, J = 4 Hz), 6.40 (s, broad, 1H, –N**H**-CH_3), 6.27 (s, broad, 1H, aromatic), 6.01 (s, broad, 1H, aromatic), 2.71 (s, 3H, NC***H***$_3$).

2.3.7. Synthesis of (4-hydroxy-2-oxidobenzaldehyde 4-ethylthiosemicarbazonato)-(2,2′-bipyridine)zinc(II) trihydrate, [Zn(bipy)(HE)]·3H_2O (**7**)

Similar to the preparation of **5**.

Yield: 0.38 g, 75%. *Anal.* Calc. for $C_{20}H_{25}N_5O_5SZn$: C, 46.83; H, 4.91; N, 13.65. Found: C, 47.09; H, 4.42; N, 13.30%. IR (KBr disc, cm^{-1}): 3400 m, 3221 m, 3064 w, 2974 m, 1603 s, 1442 m, 1336 m, 1268 m, 1227 m, 1172 m, 853 m, 799 m, 762 m, 591 m, 420 w (s, strong; m, medium; w, weak).

Characteristic ^{1}H NMR signals (DMSO-d_6, TMS, ppm): 8.61 (d, 2H, bipy, J = 4 Hz), 8.45 (d, 2H, bipy, J = 8 Hz), 8.22 (s, 1H, CH=N), 8.01 (s, broad, 2H, bipy), 7.51 (s, broad, 2H, bipy), 6.94 (d, 1H, aromatic, J = 4 Hz), 6.30 (s, broad, 1H, aromatic), 6.25 (t, 1H, –N**H**-CH_2CH_3), 6.01 (s, broad, 1H, aromatic), 3.21 (m, 2H, –NHC-**H**$_2$CH3, J = 4 Hz), 1.01 (t, 3H, –$NHCH_2$C-**H**$_3$, J = 4 Hz).

2.3.8. Synthesis of (4-hydroxy-2-oxidobenzaldehyde 4-phenylthiosemicarbazonato)-(2,2′-bipyridine)zinc(II) dihydrate, [Zn(bipy)(HP)]·2H_2O (**8**)

Similar to the preparation of **5**.

Yield: 0.44 g, 81%. *Anal.* Calc. for $C_{24}H_{23}N_5O_4SZn$: C, 53.09; H, 4.27; N, 12.90. Found: C, 53.54; H, 4.31; N, 12.55%. IR (KBr disc, cm^{-1}): 3620 w, 3327 m, 3109 w, 3070 w, 1598 m, 1484 s, 1429 m, 1313 m, 1217 m, 1172 m, 846 m, 755 m, 588 w, 568 w, 508 w, 450 w (s, strong; m, medium; w, weak).

Characteristic ^{1}H NMR signals (DMSO-d_6, TMS, ppm): 9.61 (s, broad, 1H, OH), 8.64 (d, 2H, bipy, J = 4 Hz), 8.41 (d, 2H, bipy, J = 8 Hz), 7.96 (t, 2H, bipy, J = 8 Hz), 7.76 (d, 2H, bipy, J = 8 Hz), 7.47 (t, 2H, aromatic, J = 4 Hz), 7.15 (t, 2H, aromatic, J = 8 Hz), 7.01 (s, broad, 1H, aromatic), 6.79 (t, 1H, aromatic, J = 4 Hz), 6.38 (s, broad, 1H, aromatic), 5.92 (s, broad, 1H, aromatic).

2.4. X-ray crystallography

Green crystal for complex **8** were recrystallised from dimethylformamide (DMF). The unit cell parameters and the intensity data were collected on a Bruker SMART APEX CCD diffractometer, equipped with a Mo Kα X-ray source (λ = 0.71073 Å). The APEX2 software was used for data acquisition and the SAINT software for cell refinement and data reduction. Absorption corrections on the data were made using SADABS [11]. The structures were solved and refined by SHELXL97 [12]. Molecular graphics were drawn by using XSEED [13]. Material for publication was prepared using PUBLCIF [14]. The structures were solved by direct-methods and refined by a full-matrix least-squares procedure on F^2 with anisotropic displacement parameters for non-hydrogen atoms.

2.5. Cytotoxicity assay

2.5.1. Cell culture

All the cells that were used in this study were obtained from American Type Cell Collection (ATCC) and Lonza and maintained in a 37 °C incubator with 5% CO_2 saturation. PC3 prostate adenocarcinoma cells were maintained in RPMI medium. The medium was supplemented with 10% fetus calf serum (FCS), 100 units/ml penicillin, and 0.1 mg/ml streptomycin. RWPE-1 normal prostate cells were cultured in Keratinocyte-Serum Free Medium supplemented with 100 units/ml penicillin, and 0.1 mg/ml streptomycin.

2.5.2. Cellular viability

The cell types from above were used to determine the inhibitory effect of the synthetic compounds on cell growth using the MTT assay. For measurement of cell viability, cells were seeded at a density of 1×10^5 cells/ml in a 96-well plate and incubated for 24 h at 37 °C, 5% CO_2. On the next day, cells were treated with the test agents and incubated for another 24 h. After 24 h, MTT solution at 2 mg/ml was added for 1 h. Absorbance at 570 nm were measured and recorded. The potency of cell growth inhibition for each test agent was expressed as an IC_{50} value, defined as the concentration that caused a 50% loss of cell growth. Viability was defined as the ratio (expressed as a percentage) of absorbance of treated cells to untreated cells.

2.5.3. Statistical analyses

Each experiment was performed at least two times. Results are expressed as the means value ± standard deviation (SD). Log EC_{50} calculations were performed using the built-in algorithms for dose–response curves with variable slope in Graphpad Prism software (version 4.0; GraphPad Software Inc., San Diego, CA).

2.6. Human topoisomerase I inhibition assay

The human DNA topoisomerase I inhibitory activity was determined by measuring the relaxation of supercoiled plasmid DNA pBR322. For measurement of human topoisomerase I activity, the reaction mixtures were comprised of 10 mM Tris–HCl, pH 7.5, 100 mM NaCl, 1 mM phenylmethylsulfonyl fluoride (PMSF), α-toluenesulfonyl fluoride, and 1 mM 2-mercaptoethanol, 0.25 μg plasmid DNA pBR322, 1 unit of human DNA topoisomerase I, and metal complex with final concentration of 40 μM. All reactions were conducted at a final volume of 20 μl and were prepared on ice. Upon enzyme addition, reaction mixtures were incubated at 37 °C for 30 min. The reactions were terminated by the addition of 2 μl of 10% sodium dodecyl sulfate (SDS) and then followed by 3 μl of dye solution comprising 0.02% bromophenol blue and 50% glycerol. SDS is required to observe a linear DNA fragment and to denature topoisomerase I, preventing further functional enzymatic activity. The mixtures were applied to 1.2% agarose gel and electrophoresed for 5 h at 33 V with running buffer of Tris–acetate EDTA (TAE) at pH 8.1. The gel was stained, destained, and photographed under UV light using a Syngene Bio Imaging system and the digital image was viewed with Gene Flash software.

In the human DNA topoisomerase I inhibition condition study, the same protocol was applied. This study is designed to deduce the mode of action of metal complex in the human DNA topoisomerase I inhibition study. The sequence of addition of the main components (human DNA topoisomerase I, plasmid DNA pBR322, and metal complex) was varied. For the first condition, human DNA topoisomerase I with the metal complex was incubated at 37 °C for 30 min before the addition of DNA. This mixture was incubated for another 30 min at the same temperature after the addition of DNA. As for the second condition, the metal complex and DNA was incubated for 30 min at 37 °C first, and then followed by the addition of topoisomerase I. This mixture was incubated for another 30 min at 37 °C after the addition of topoisomerase I.

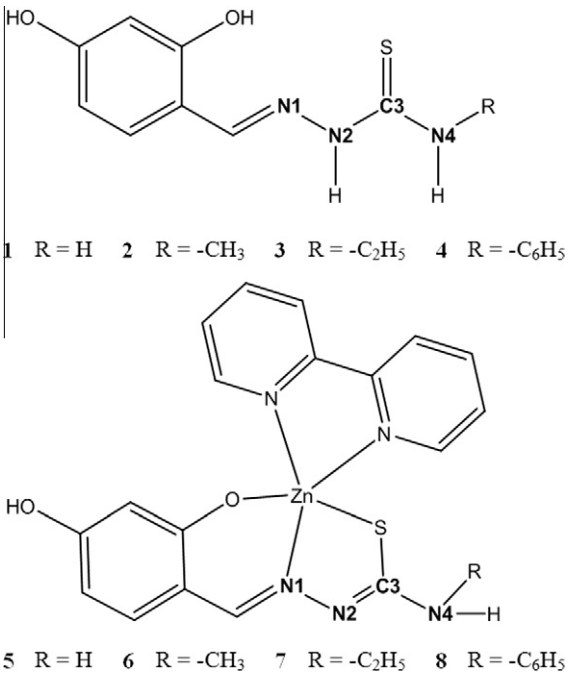

Fig. 1. Proposed structures for all the compounds.

3. Results and discussion

3.1. Synthesis of ligands and complexes

Proposed structures for all the compounds with IUPAC numbering scheme are shown in Fig. 1. Results from partial elemental analyses are in good agreement with the proposed formulation of Zn(bipy)L where bipy = 2,2′-bipyridine and L is the doubly deprotonated thiosemicarbazones. All the complexes are yellow in appearance except **8**, which is yellowish green. Ligands **1**–**4** are prepared in high yield from the condensation of 2,4-dihydroxybenzaldehyde with the respective thiosemicarbazides while the complexes are prepared in high yield by refluxing zinc acetate dihydrate, 2,2′-bipyridine and the thiosemicarbazones in ethanol. All the complexes were isolated with the ligands coordinating in the thiolate form. In the absence of acetate, reaction of similar ligands with zinc chloride has led to formation of a dinuclear complex with the thiosemicarbazone moiety coordinating in the thione form [15].

Complexes **6** and **7** are soluble in methanol, DMF and DMSO. Complexes **5** and **8** are insoluble in common polar and non-polar solvents but are soluble in DMF and DMSO. None of the complexes are sufficiently soluble in DMSO for acquisition of ^{13}C NMR spectra.

3.2. Crystal structures of [Zn(bipy)(HP)]·2H$_2$O (**8**)

Complex **8** crystallized into an orthorhombic lattice with space group symmetry *Pbca*. The perspective view of the complex with numbering scheme is shown in Fig. 2. Crystal data and structure refinement parameters for compound **8** are shown in Table 1. Selected bond lengths and angles are presented in Table 2.

The complex is mononuclear and five coordinated with the doubly deprotonated thiosemicarbazone as a tridentate ligand coordinating through the phenolic oxygen, azomethine nitrogen and thiolate sulfur while 2,2′-bipyridine as the *N,N′*-bidentate ligand. The trigonality index τ of 0.57 for **8** indicates that the coordination geometry around zinc is intermediate between trigonal bipyramidal and square pyramidal geometries and is better described as trigonal bipyramidal distorted square based pyramid (TBDSBP). This value is similar to the value reported for [Zn(bipy)L] where L = salicylaldehyde 4-phenylthiosemicarbazone [16].

The deviation from an ideal stereochemistry may be due to the restricted bite angle imposed by both the thiosemicarbazone and bipy ligands [16]. The bite angle around the metal for 2,2′-bipyridine of 78.19(6)° may be considered larger when compared with an average value of 77° reported in the literature for zinc complexes with 2,2′-bipyridine [17]. Zn–$N_{azomethine}$ bond length of 2.0535(14) Å is shorter than the Zn–N_{bipy} bond lengths of 2.1220(15) and 2.0954(15) Å. This indicates that the azomethine nitrogen is coordinated more strongly to zinc compared to the bipyridine nitrogen and the thiosemicarbazone moiety dominates equatorial bonding. The imine bond formation is evidenced from N1–C7 and N2–C9 distances of 1.290(2) Å and 1.306(2) Å. The C–N bond length of 1.306(2) Å and C–S bond length of 1.7500(17) is similar to those reported for coordination of thiosemicarbazone in the thiolate form [16,18].

Hydrogen bonding interactions for complex **8** is shown in Figs. 3 and 4. Hydrogen bonding parameters are shown in Table 3.

The mononuclear complexes form a zig–zag chain through N3–H3—O2 hydrogen bonding as shown in Fig. 3 due to the presence of uncoordinated hydroxyl group. The water molecules in the crystal lattice play an important role in the crystal packing. In addition to the direct intermolecular hydrogen bonding (N3–H3···O2) between the mononuclear complexes, water molecules in the crystal lattice help to bridge the adjacent mononuclear complexes into a three-dimensional network through a series of complex hydrogen bonding interactions (O2–H2···O2w, O1w–H11···O1, O2w–H21···N2^{i} and O2w–H22···O1w^{ii}) as shown in Fig. 4. These observations underscore the important role played by the uncoordinated hydroxyl group in hydrogen bonding interactions which is not observed in metal complexes derived from salicylaldehyde N(4)-substituted thiosemicarbazone [5b,d,19].

The packing of the molecules is shown in Fig. 5. The molecules in the crystal lattice are stabilized by combination of hydrogen bonding and π–π interactions between aromatic rings. The expected offset or slipped stacking interactions were observed because of no substantial overlap of aromatic surface area. π stacking becomes favorable with increase in ring numbers [20].

3.3. Infrared and electronic spectra

Important IR bands for the ligands and complexes are given in Table S1 (Supplementary material). The bands from 3331 to 3478 cm^{-1} are assigned to ν(O–H) of the free ligands [5a]. Meanwhile, the bands from 3248 to 3342 cm^{-1} are assigned to ν(N(4)–H) [5]. The bands at around 3127–3174 cm^{-1} are assigned to ν(N(2)–H) [16,21]. Thiosemicarbazones are known to exhibit thione–thiol tautomerization. The absence of any band around 2600–2800 cm^{-1} ν(S–H) indicates that in the solid form, all the ligands exist in the thione form [3a,22].

In contrast to complexes of salicylaldehyde thiosemicarbazone, the bands around 3380 cm^{-1} due to ν(O–H) are still seen in the spectra of all the complexes indicating that only one of the phenolic oxygen atoms from each thiosemicarbazone ligand is deprotonated and involved in coordination. The disappearance of the ν(N(2)–H) band in the spectra of all the complexes indicates the deprotonation of the hydrazinic proton which is in accordance with coordination of the sulfur atom in the thiolate form [5a,b,d,f,16,19,23].

Coordination of the azomethine nitrogen is confirmed by the shift of ν(C=N) from 1620–1629 to 1598–1604 cm^{-1}. Evidence of coordination of the thiolate sulfur is further supported by the decrease in frequency of the thioamide band found at around 1323–1379 and 838–868 cm^{-1} to 1273–1316 and 799–849 respectively as reported by Campbell [24]. The bands from 1231 to 1264 cm^{-1} due to ν(C–O) decrease by 20–40 cm^{-1} upon coordina-

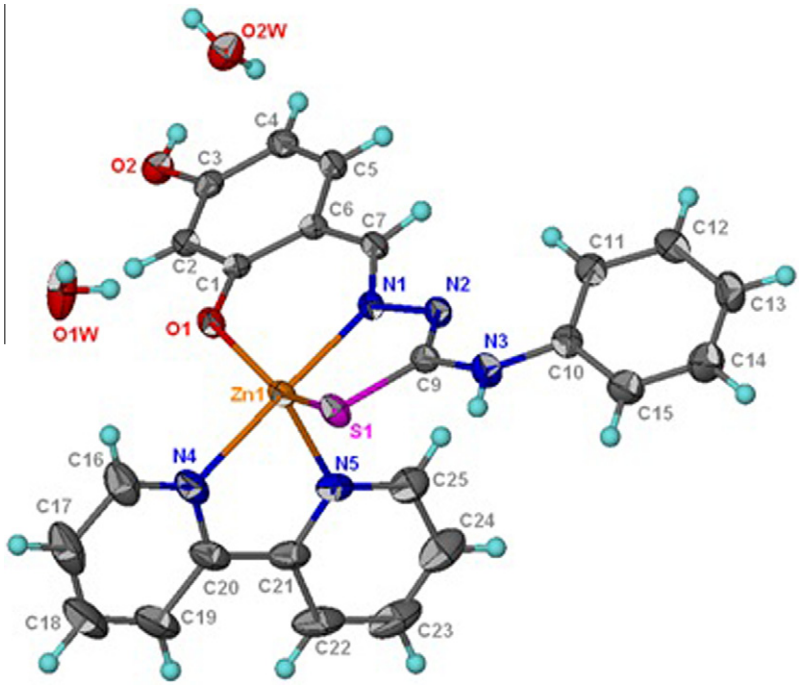

Fig. 2. Thermal ellipsoid [13] plot of **8** drawn at the 70% probability level. Hydrogen atoms are drawn as spheres of arbitrary radii.

Table 1
Crystal data and structure refinement parameters for compound **8**.

Compound	[Zn(bipy)(HP)·2H$_2$O (**8**)
Empirical formula	$C_{24}H_{23}N_5O_4SZn$
Formula weight	542.90
Crystal system	Orthorhombic
Space group	*Pbca*
Unit cell dimensions	
a (Å)	17.9569(9)
b (Å)	12.9769(7)
c (Å)	20.4834(11)
β (°)	90
V (Å^3)	4773.1(4)
Z	8
F(000)	2240
D_{calc} (mg m^{-3})	1.511
Absorption coefficient, μ (mm^{-1})	1.16
T (K)	100(2)
Crystal size (mm)	0.35 × 0.25 × 0.15
Reflections collected	25918
Independent reflections (R_{int})	5481(0.029)
Data/restraints/parameters	5481/20/350
$R[F^2 > 2\sigma(F^2)]$	0.028
$wR(F^2)$	0.076
S	1.03
Largest differencepeak and hole (e Å^{-3})	0.34 and −0.33

Table 2
Selected bond lengths (Å) and angles (°) for [Zn(bipy)(HP)]·2H$_2$O (**8**).

Bond lengths		Bond angles	
Zn1–O1	2.0069(12)	O1–Zn1–N1	89.21(5)
Zn1–N1	2.0535(14)	O1–Zn1–N5	109.88(6)
Zn1–N5	2.0954(15)	N1–Zn1–N5	100.24(6)
Zn1–N4	2.1220(15)	O1–Zn1–N4	91.39(5)
Zn1–S1	2.3657(5)	N1–Zn1–N4	178.43(6)
S1–C9	1.7500(17)	N5–Zn1–N4	78.19(6)
O1–C1	1.327(2)	O1–Zn1–S1	144.46(4)
O2–C3	1.364(2)	N1–Zn1–S1	82.23(4)
N1–C7	1.290(2)	N5–Zn1–S1	105.58(4)
N1–N2	1.3951(19)	N4–Zn1–S1	98.10(4)
N2–C9	1.306(2)	C9–S1–Zn1	92.65(6)
N3–C9	1.367(2)	C1–O1–Zn1	126.12(10)
N3–C10	1.408(2)		
N4–C16	1.332(3)		
N4–C20	1.350(3)		
N5–C25	1.338(3)		

tion. This confirms the coordination of the phenolic oxygen to zinc [5b,16].

The *ν*(N–N) band of the thiosemicarbazones is found at 1121–1166 cm^{-1}. The increase in the frequency of this band upon complexation is due to the increase in the double bond character offsetting the loss of electron density via donation to the metal and is a confirmation of the coordination of the ligand through the azomethine nitrogen atom [16]. The appearance of new *ν*(Zn–N) bands in the range of 420–450 cm^{-1} confirms the coordination through azomethine and polypyridyl nitrogens. Coordination through phenolic oxygen is confirmed by the presence of a new *ν*(Zn–O) band in the spectra of the complexes at 551–591 cm^{-1} [16]. The mode of coordination for the ligands and complexes determined by IR spectra is in good agreement with the crystal structures of complexes **5** and **8**. Complexes **5–8** have very similar IR spectra, this indicates that they share the similar mode of coordination.

Electronic spectral assignments for the ligands and their zinc(II) complexes in DMF are presented in Table 4. All the ligands and the Zn(II) complexes have a ring (phenolic and diimine) π–π* band at around 37593 cm^{-1} [5a]. No significant red shift is observed for these bands upon complexation [25]. All the free thiosemicarbazones also have two bands at around 32985 and 29411 cm^{-1} due to n–π* transition of azomethine and thioamide function, respectively.

Upon complexation, the n–π* band of the thioamide function is shifted above 30000 cm^{-1} due to thioenolization and merges with the azomethine n–π* band at around 31348 cm^{-1} [25]. Thioenolization causes the weakening of the C=S bond attributed to the loss in double bond character. A moderately intense band in the range 26455–27473 cm^{-1}, found only in the spectra of the complexes, is assigned to Zn(II) → S metal to ligand charge transfer band (MLCT)

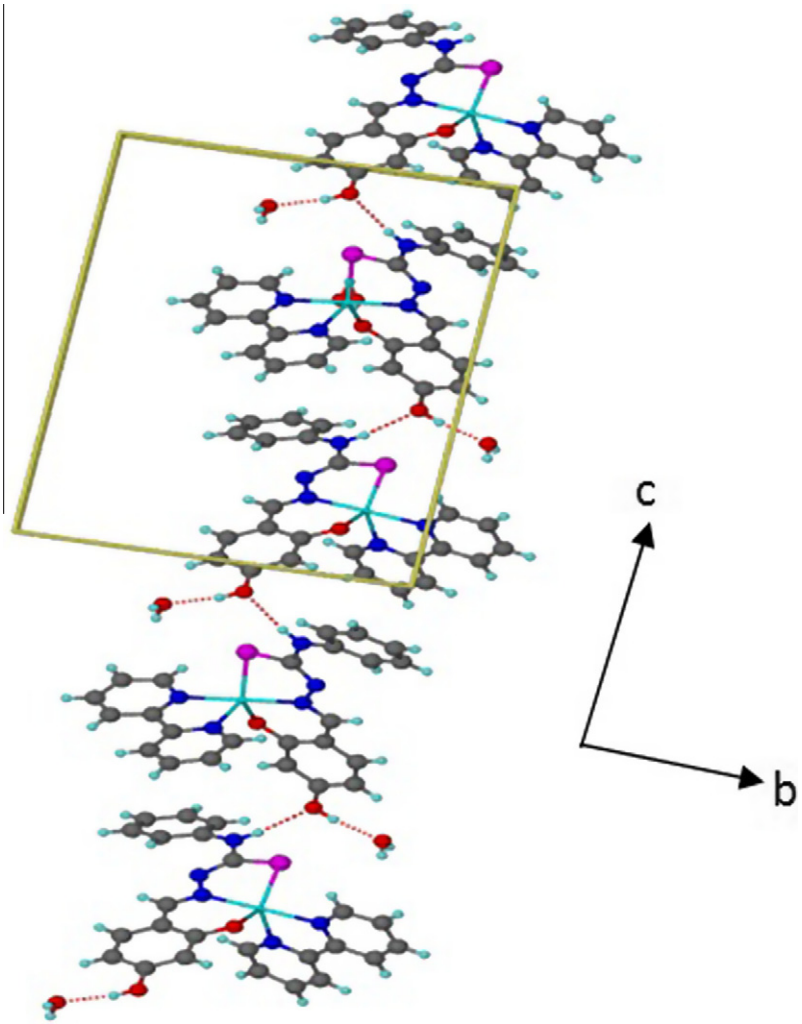

Fig. 3. Zig–zag chain formed from N3–H3—O2 hydrogen bonding interactions for complex **8**.

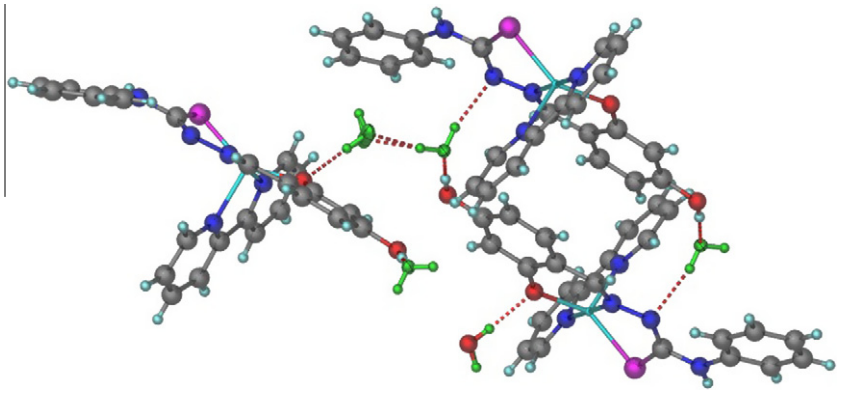

Fig. 4. Water molecules (green) bridging the adjacent mononuclear complexes into a three-dimensional network through hydrogen bonding. (For interpretation of references to color in this figure legend, the reader is referred to the web version of this article.)

[16,25]. The MLCT band for Zn(II) → O shows line broadening that runs into the visible part of the spectrum. However, the maxima of this band is not observed probably due to the overlapping with the low energy side of Zn(II) → S transitions [16]. The absence of bands below 22 000 cm^{-1} due to d–d transitions is in accordance with the d^{10} electron configuration of Zn(II) ion [16,26].

3.4. ^{1}H and ^{13}C NMR spectra

All the thiosemicarbazones ligands have a sharp signal in the region of 11.14–11.79 ppm that integrates to one proton which is assigned to N(2)H. The presence of hydrogen bonds decrease the electron density about N(2) protons and hence move the absorp-

Table 3
Hydrogen-bond geometry (Å, °) for [Zn(bipy)(HP)]·2H$_2$O (**8**).

D–H···*A*	*D*–H	H···*A*	*D*···*A*	*D*–H···*A*
O2–H2···O2w	0.84(1)	1.84(1)	2.66(1)	172(2)
O1w–H11···O1	0.84(1)	1.91(1)	2.72(1)	161(3)
O2w–H21···N2^{i}	0.84(1)	2.15(1)	2.94(1)	159(3)
O2w–H22···O1w^{ii}	0.83(1)	1.88(2)	2.70(1)	172(3)
N3–H3···O2^{iii}	0.87(1)	2.19(1)	3.04(1)	171(2)

Symmetry codes: (i) $-x+1, -y+2, -z+1$; (ii) $-x+1, y+1/2, -z+3/2$; (iii) $x+1/2, -y+3/2, -z+1$.

Table 4
Electronic spectral assignments (cm^{-1}) for the ligands and their zinc(II) complexes in DMF.

Compound	π–π*	n–π*	MLCT
H_3T (**1**)	37593	33003, 29411	
H_3M (**2**)	37593	33003, 29411	
H_3E (**3**)	37593	32895, 29240	
H_3P (**4**)	37453	32680, 28409	
[Zn(bipy)(HT)] (**5**)	37736	31250	27473
[Zn(bipy)(HM)]·3H$_2$O (**6**)	37736	31447	27027
[Zn(bipy)(HE)]·3H$_2$O (**7**)	37736	31348	27248
[Zn(bipy)(HP)]·2H$_2$O (**8**)	37593	31152	26455

tion down field [27]. In the spectra of the thiosemicarbazones, the signals for the phenolic protons are found at 9.74–9.93 ppm [28]. Meanwhile, the azomethine protons of all the ligands are found as a sharp singlet at 8.20–8.34 ppm due to the absence of any neighboring protons. The absence of signals at around 4 ppm, due to the –SH (thiol) group, indicates that all the ligands exist in the thione form. The signal for N(4)H appears in the region of 7.65–8.72 ppm and the value is highly dependent on the substituent groups. It is noteworthy that the N(4)H protons for compounds **2** and **3** exist as a doublet with a coupling constant $J = 4$ Hz due to the $^{3}J_{H-H}$ splitting by the alkyl group attached to the N(4) atom. This sort of coupling through a nitrogen bond is seldom seen due to N–H exchange or quadrupole broadening [27]. The absence of the N(2)H peak in the spectra of all the complexes indicates the deprotonation of the hydrazinic proton and supports the coordination of sulfur in the thiolate form. Coordination of the azomethine nitrogen is confirmed by the shifting of the –CH=N signal from 8.20–8.34 ppm in the free ligands to 8.18–8.27 ppm in the spectra of the complexes. Even though the –CH=N signal normally shifts downfield upon complexation, irregularities in this trend is not uncommon [5f]. The –CH=N and N(4)H signals for complex **8** are not observed due to overlapping with the bipyridine protons signals at around 8.64–8.40 ppm. The formation of ternary complexes is shown by the presence of four signals with different multiplicity in the region of 7.48–8.62 ppm ascribed to the coordinated 2,2′-bipyridine ligand.

All ligands show a carbon signal in the region 175.57–177.61 ppm due to C=S. Each ligand shows two signals that correspond to C–O are observed in the region of 158.40–161.21 ppm. The formation of the Schiff base is confirmed by the presence of the azomethine carbon signal (C=N) at around 141 ppm in the spectra of all the ligands. The signals due to aromatic carbons are found at 102.81–139.64 ppm. Compound **3** has an additional peak

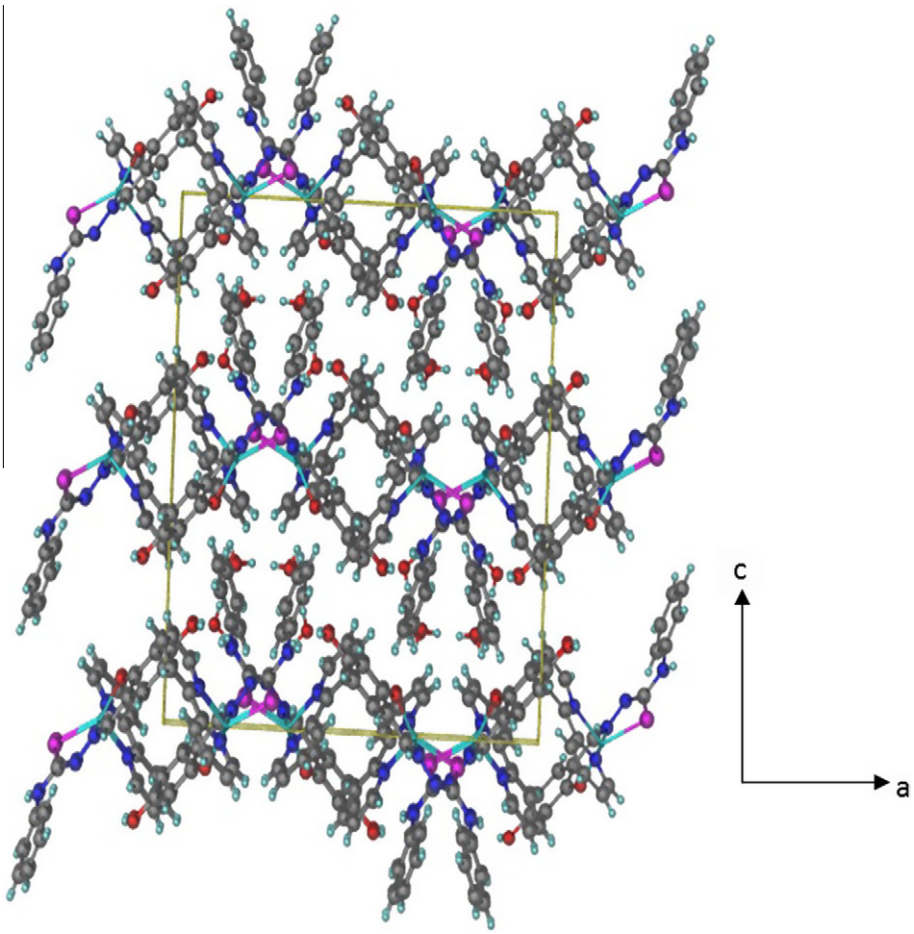

Fig. 5. Unit cell packing diagram of **8** view along *b* axis.

due to N–**C**H_3 at 31.28 ppm while compound **4** has two signals at 15.21 and 32.20 due to NCH_2**C**H_3 and N**C**H_2–, respectively. The total numbers of C signals in the spectra of all ligands are in agreements with the proposed structures. The values reported are similar to those in the literature [22]. None of the complexes were sufficiently soluble in DMSO to record acceptable ^{13}C spectra.

3.5. Cytotoxic activity

The free ligands and the complexes were tested on PC3 and RWPE-1 cells, respectively. Prostate cancer cells were chosen in this study because the level of topoisomerase I in prostate tumors was known to increase by 2- to 10-fold, compared with benign hyperplastic prostate tissue from the same patients [29]. This makes prostate carcinoma cells a good model for studying the cytotoxicity of compounds that were designed to target topoisomerase I.

After 24 h, cell viability was determined by the MTT assay. Test agents decreased cell proliferation in a concentration dependent manner. These dose titration curves allowed the determination IC_{50} for the test agents towards different cell lines (Table 5). All the ligands are non-cytotoxic within the tested concentrations. The complexes show very good cytotoxicity towards PC3 with concentrations in the range of 0.84–2.24 μM with the exception for complex **5** which is non-cytotoxic. This underscores the importance of a hydrophobic substituent at the N(4) position in modulating the cytotoxicity of the metal complexes. Interestingly, the cytotoxicity of the complexes towards PC3 decreases in the following order: **8** > **7** > **6**. This indicates that the cytotoxicity of the complexes improves with the increase in hydrophobicity of the N(4) substituents from methyl to ethyl and phenyl. Similar observation has been reported by Rebolledo et al., where palladium(II) complexes of 2-benzoylpyridine thiosemicarbazone with a phenyl substituent at the N(4) is the most cytostatic compared to the methyl substituted and non-substituted derivatives [10]. In addition, complexes **6**–**8** also show higher toxicity towards cancer cells (PC3) compared with normal cells (RWPE-1). The selectivity of these zinc complexes could be attributed to the distinct difference between the zinc concentration in normal and cancerous prostate cells. Since normal prostate cells are known to have higher zinc level compared with the cancerous cells, this may resulting in the lower uptake of the zinc complexes into the normal cells that are almost saturated with zinc. Therefore, the zinc complexes are less toxic to the normal cells. However, further studies on drug uptakes are required to confirm our hypothesis. It is noteworthy that complex **8**, is a hundred times more toxic towards cancer cells compared with normal cells. Since the cancerous cells are known to have higher expressions of topoisomerase I, the outstanding cytotoxicity of complex **8** could be attributed to its ability in inhibiting topoisomerase I as we observed here.

Table 5
IC_{50} values (μM) at 10 000 cells per well for the complexes on PC3 and RWPE-1 cells, respectively.

Sample	PC3		RWPE-1	
	IC_{50}	SEM	IC_{50}	SEM
1	NC		NC	
2	NC		NC	
3	NC		NC	
4	NC		NC	
5	NC		NC	
6	2.24	0.358	76.06	3.546
7	1.56	0.248	50.03	2.348
8	0.84	0.267	85.63	4.356

NC = non-cytotoxic.

3.6. Topoisomerase I inhibition assay

Topoisomerases are important nuclear enzymes that modify the topological state of DNA by catalyzing the relaxation of negative supercoils and the negative supercoiling of DNA [30]. Those enzymes that cleave only one strand of the DNA are defined as type I whereas topoisomerases that cleave both strands to generate a staggered double-strand break are known as type II topoisomerases [31]. These enzymes play essential roles in mitosis, particularly in DNA transcription and replication [32]. Topoisomerases have been identified as important targets in cancer chemotherapy and microbial infections [33]. In fact, topoisomerase I inhibitors are quoted as having a wide range of antitumor activities and are among the most widely used anticancer drugs clinically [34]. However, very few metal complexes have been reported to inhibit topoisomerases and even fewer zinc complexes have been reported to inhibit topoisomerase I and II [35].

In our DNA relaxation assay, one unit of human topo I can completely convert all the supercoiled plasmid pBR322 (4.4 kb) to fully relaxed topoisomer, which is the completely unwound covalently bonded closed circular DNA (Fig. 6, lane L7). This is found in the slowest moving DNA band (labeled Form II) which contains the fully relaxed closed circular pBR322 and the originally present, small amount of nicked DNA. No cleavage or unwinding of the DNA was observed when pBR322 was incubated with 40 μM of complexes **5–8** alone (Fig. 6, lanes L2–L5). As can be seen from Fig. 6 (lane L10) only complex **8**, Zn(bipy)(HP) is capable of inhibiting topo I with total disappearance of the nicked band (containing nicked and fully relaxed DNA).

As a preliminary investigation into the mechanism of action of the above topo I inhibition, we used three variations of mixing the DNA, topo I and the zinc complex **8** (at 40 μM) for the topo I inhibition assay. When the three components are mixed simultaneously, there is slight inhibition of topo I as seen by the presence of the fastest moving band with low intensity (Form I) which consists of supercoiled DNA and poorly relaxed DNA (Fig. 7, lane L5). The bands of topoisomers with different degrees of relaxation can also be seen in between Form I and Form II. Secondly, when complex **8** was incubated first with topo I before the addition of DNA, the intensity of the fastest moving band is the highest with almost total disappearance of the slowest moving band (Form II), suggesting that almost total inhibition of topo I (Fig. 7, lane L6). Finally, when the DNA is first incubated with the zinc complex for 30 min before adding the topo I (Fig. 7, lane L7), the fastest moving band (Form I) almost totally disappears. The intensity of Form II is slightly lower compared to the control in lane L4. The presence of relaxed topoisomers just below the fully relaxed topoisomer band (Form II) indicates that inhibition of topo I is less than the two

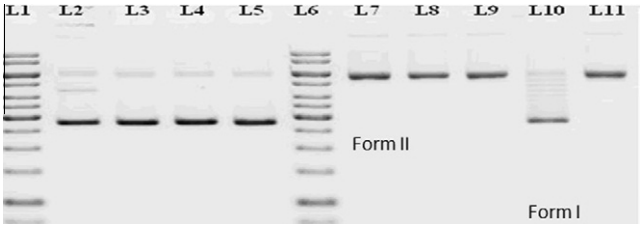

Fig. 6. Human topoisomerase I inhibition assay by gel electrophoresis. Electrophoresis results of incubating human topoisomerase I (1 unit/21 μl) with pBR322 in the absence or presence of 40 μM of complex: lanes 1 and 6, gene ruler 1 kb DNA ladder; lane 2, DNA + 40 μM **7** (control); lane 3, DNA + 40 μM **6** (control); lane 4, DNA + 40 μM **8** (control); lane 5, DNA + 40 μM **5** (control); lane 7, DNA + 1 unit human topoisomerase I (control); lane 8, DNA + 40 μM **7** + 1 unit human topoisomerase I; lane 9, DNA + 40 μM **6** + 1 unit human topoisomerase I; lane 10, DNA + 40 μM **8** + 1 unit human topoisomerase I; lane 11, DNA + 40 μM **8** + 1 unit human topoisomerase I.

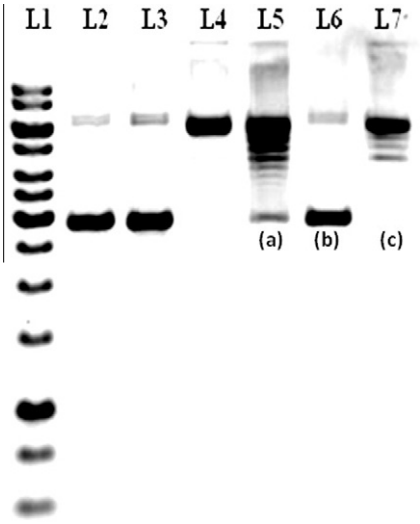

Fig. 7. Effect of sequence of mixing for the human topoisomerase I inhibition assay of complex **8**. Electrophoresis results of incubating human topoisomerase I (1 unit/21 μL) with pBR322: lane 1, 1 kb DNA ladder; lane 2, plasmid DNA pBR 322 (control); lane 3, DNA + 40 μM complex (control); lane 4, DNA + 1 unit human topoisomerase I (control); (a) all components mixed at the same time; lane 5, DNA + 40 μM complex + 1 unit human topoisomerase I; (b) complex + TopoI incubated for 30 min first before DNA is added; lane 6, DNA + 40 μM complex + 1 unit human topoisomerase I; (c) complex + DNA incubated for 30 min first before TopoI is added; lane 7, DNA + 40 μM complex + 1 unit human topoisomerase I.

methods of mixing earlier. Therefore, two pathways of topoisomerase inhibitions are suggested, one involves the binding of complex to DNA while the other involves the binding to topoisomerase. By comparing lanes L6 and L7, we can infer that since greater inhibition of topo I is observed when the complex is incubated with topo first, the inhibition process involving the binding of the complex to the topoisomerase enzyme may be a more dominant pathway. However, further investigation is crucial to confirm this.

4. Conclusions

Results from biological tests indicate that the nature of the N(4) substituent plays a crucial role in determining the selectivity and potency of zinc(II) complexes of N(4)-substituted thiosemicarbazones. Complex **8** may hold the key in developing new class of thiosemicarbazone based anticancer agent with highly selective toxicity towards prostate cancer.

Acknowledgements

The authors acknowledge the support from UMRG(RG148-11AFR) from UM and FRGS(FP044-2010B) from MOSTI.

Appendix A. Supplementary data

CCDC 865233 contains the supplementary crystallographic data for compound **8**. These data can be obtained free of charge via http://www.ccdc.cam.ac.uk/conts/retrieving.html, or from the Cambridge Crystallographic Data Centre, 12 Union Road, Cambridge CB2 1EZ, UK; fax: (+44) 1223-336-033; or e-mail: deposit@ccdc.cam.ac.uk. Supplementary data associated with this article can be found, in the online version, at http://dx.doi.org/10.1016/j.poly.2012.03.014.

References

[1] (a) A.E. Liberta, D.X. West, Biometals 5 (1992) 121;
(b) H. Beraldo, D. Gambino, Mini-Rev. Med. Chem. 4 (2004) 31.
[2] (a) S. Attia, J. Kolesar, M.R. Mahoney, H.C. Pitot, D. Laheru, J. Heun, W. Huang, J. Eickhoff, C. Erlichman, K.D. Holen, Invest. New Drugs 26 (2008) 369;
(b) O.M. Odenike, R.A. Larson, D. Gajria, M.E. Dolan, S.M. Delaney, T.G. Karrison, M.J. Ratain, W. Stock, Invest. New Drugs 26 (2008) 233;
(c) B. Ma, B.C. Goh, E.H. Tan, K.C. Lam, R. Soo, S.S. Leong, L.Z. Wang, F. Mo, A.T.C. Chan, B. Zee, T. Mok, Invest. New Drugs 26 (2008) 169.
[3] (a) Z. Afrasiabi, E. Sinn, J. Chen, Y. Ma, A.L. Rheingold, L.N. Zakharov, N. Rath, S. Padhye, Inorg. Chim. Acta 357 (2004) 271;
(b) J. Chen, Y.W. Huang, G. Liu, Z. Afrasiabi, E. Sinn, S. Padhye, Y. Ma, Toxicol. Appl. Pharmacol. 197 (2004) 40;
(c) L. Wei, J. Easmon, R.K. Nagi, B.D. Muegge, L.A. Meyer, J.S. Lewis, J. Nucl. Med. 47 (2006) 2034;
(d) V.A. Rao, S.R. Klein, K.K. Agama, E. Toyoda, N. Adachi, Y. Pommier, E.B. Shacter, Cancer Res. 69 (2009) 948.
[4] (a) S. Adsule, V. Barve, D. Chen, F. Ahmed, Q.P. Dou, S. Padhye, F.H. Sarkar, J. Med. Chem. 49 (2006) 7242;
(b) V. Barve, F. Ahmed, S. Adsule, S. Banerjee, S. Kulkarni, P. Katiyar, C.E. Anson, A.K. Powell, S. Padhye, F.H. Sarkar, J. Med. Chem. 49 (2006) 3800.
[5] (a) D.X. West, A.E. Liberta, S.B. Padhye, R.C. Chikate, P.B. Sonawane, A.S. Kumbhar, R.G. Yerande, Coord. Chem. Rev. 123 (1993) 49;
(b) L. Latheef, M.R.P. Kurup, Spectrochim. Acta, Part A 70 (2008) 86;
(c) L. Latheef, E. Manoj, M.R.P. Kurup, Acta Crystallogr., Sect. C 62 (2006) 16;
(d) E.B. Seena, M.R.P. Kurup, Polyhedron 26 (2007) 829;
(e) E.B. Seena, M.R.P. Kurup, E. Suresh, J. Chem. Crystallogr. 38 (2008) 93;
(f) T.S. Lobana, R. Sharma, G. Bawa, S. Khanna, Coord. Chem. Rev. 253 (2009) 977.
[6] X. Zhu, C. Wang, Z. Lu, Y. Dang, Transition Met. Chem. 22 (1997) 9.
[7] (a) B.L. Vallee, D.S. Auld, Biochemistry 29 (1990) 5647;
(b) J.H. Waterborg, C.M.A. Kuyper, J. Biochem. 92 (1982) 1655.
[8] (a) C.A. Mawson, M.I. Fischer, Can. J. Med. Sci. 30 (1952) 336;
(b) G.R. Schrodt, T. Hall, W.F. Whitmore Jr., Cancer 17 (1964) 1555;
(c) K. Boddy, B.W. East, P.C. King, R.W. Simpson, R. Scott, Br. J. Urol. 42 (1970) 475;
(d) L.C. Costello, Y. Liu, R.B. Franklin, M.C. Kennedy, J. Biol. Chem. 272 (1997) 28875;
(e) V.Y. Zaichick, T.V. Sviridova, S.V. Zaichick, Int. Urol. Nephrol. 29 (1997) 565;
(f) P. Feng, J.Y. Liang, T.L. Li, Z.X. Guan, J. Zou, R.B. Franklin, L.C. Costello, Mol. Urol. 4 (2000) 31;
(g) R.G. Uzzo, P. Leavis, W. Hatch, V.L. Gabai, N. Dulin, N. Zvartau, V.M. Kolenko, Clin. Cancer Res. 8 (2002) 3579;
(h) R.B. Franklin, P. Feng, B. Milon, M.M. Desouki, K.K. Singh, A. Kajdacsy-Balla, O. Bagasra, L.C. Costello, Mol. Cancer 4 (2005) 32.
[9] (a) D. Kovala-Demertzi, P.N. Yadav, J. Wiecek, S. Skoulika, T. Varadinova, M.A. Demertzis, J. Inorg. Biochem. 100 (2006) 1558;
(b) D. Kovala-Demertzi, A. Alexandratos, A. Papageorgiou, P.N. Yadav, P. Dalezis, M.A. Demertzis, Polyhedron 27 (2008) 2731.
[10] A.P. Rebolledo, M. Vieites, D. Gambino, O.E. Piro, E.E. Castellano, C.L. Zani, E.M. Souza-Fagundes, L.R. Teixeira, A.A. Batista, H. Beraldo, J. Inorg. Biochem. 99 (2005) 698.
[11] G.M. Sheldrick, SADABS, University of Gottingen, Germany, 1996.
[12] G.M. Sheldrick, Acta Crystallogr., Sect. A 64 (2007) 112.
[13] L.J. Barbour, J. Supramol. Chem. 1 (2001) 189.
[14] S.P. Westrip, publCIF, in preparation.
[15] K.W. Tan, C.H. Ng, M.J. Maah, S.W. Ng, Acta Crystallogr., Sect. E 65 (2009) m569.
[16] E.B. Seena, M.R.P. Kurup, Spectrochim. Acta, Part A 69 (2008) 726.
[17] C.G. Zhang, C. Janiak, J. Chem. Crystallogr. 31 (2001) 29.
[18] T. Bal-Demirci, Polyhedron 27 (2008) 440.
[19] E.B. Seena, M.R.P. Kurup, Polyhedron 26 (2007) 3595.
[20] C. Janiak, J. Chem. Soc., Dalton (2000) 3885.
[21] T.A. Reena, M.R.P. Kurup, Spectrochim. Acta, Part A 76 (2010) 322.
[22] P. Bindu, M.R.P. Kurup, T.R. Satyakeerty, Polyhedron 18 (1998) 321.
[23] M.D.C. Aguirre, J. Borrás, A. Castiñeiras, J.M. Garcîa-Monteagudo, I. Garcîa-Santos, J. Niclõs, D.X. West, Eur. J. Inorg. Chem. (2006) 1231.
[24] M.J.M. Campbell, Coord. Chem. Rev. 15 (1975) 279.
[25] J.K. Swearingen, D.X. West, Transition Met. Chem. 25 (2000) 241.
[26] M.R.P. Kurup, L. Latheef, E. Manoj, Polyhedron 26 (2007) 4107.
[27] D.X. West, L.J. Ackerman, P.E. Fanwick, M.A. Green, E. John, W.E. Running, J.K. Swearingen, J.W. Webb, Polyhedron 18 (1999) 2759.
[28] I. Piantanida, I. Dilovic, M. Rubcic, V. Vrdoljak, S.K. Pavelic, M. Kralj, M. Cindric, Bioorgan. Med. Chem. 16 (2008) 5189.
[29] I. Husain, J.L. Mohler, H.F. Seigler, J.M. Besterman, Cancer Res. 54 (1994) 539.
[30] S.M. Hecht, X.Y. Wang, L.K. Wang, W.D. Kingsbury, R.K. Johnson, Biochemistry 37 (1998) 9399.
[31] (a) J.C. Wang, Nat. Rev. Mol. Cell Biol. 3 (2002) 430;
(b) J.C. Wang, Sci. Am. 247 (1982) 94;
(c) J.J. Champoux, Proc. Natl. Acad. Sci. U.S.A. 99 (2002) 11998.
[32] J.L. Nitiss, J.C. Wang, Mol. Pharmacol. 50 (1996) 1095.

[33] D.S. Pandey, S.K. Singh, S. Joshi, A.R. Singh, J.K. Saxena, Inorg. Chem. 46 (2007) 10869.
[34] (a) M.L. Rothenberg, C.D. Blanke, Semin. Oncol. 26 (1999) 632;
(b) M.L. Rothenberg, Ann. Oncol. 8 (1997) 837;
(c) F. Zunino, G.L. Beretta, P. Perego, Expert Opin. Ther. Targets 12 (2008) 1243;
(d) S. Dallavalle, S. Gattinoni, S. Mazzini, L. Scaglioni, L. Merlini, S. Tinelli, G.L. Beretta, F. Zunino, Bioorg. Med. Chem. Lett. 18 (2008) 1484.
[35] (a) E. Kimura, E. Kikuta, T. Koike, J. Inorg. Biochem. 79 (2000) 253;
(b) N.N. Chuang, C.L. Lin, H.K. Chen, Comp. Biochem. Phys. B 114 (1996) 145;
(c) C.H. Ng, H.L. Seng, S.T. Von, K.W. Tan, M.J. Maah, S.W. Ng, R.N.Z.R.A. Rahman, I. Caracelli, Biometals 23 (2010) 99.